Melting of square crystals in two dimensions

Thomas A. Weber
Division of Information Systems, National Science Foundation, Washington, D.C. 20550

Frank H. Stillinger
AT&T Bell Laboratories, Murray Hill, New Jersey 07974
(Received 23 June 1993)

A 2500-particle molecular-dynamics simulation has been carried out for a two-dimensional continuum model whose classical ground state is a crystal with square symmetry. The interaction potential comprises two-body and three-body contributions. Evidence from both heating and cooling sequences indicates that the crystal-liquid transition is a conventional first-order phase change. Inherent structures (potential-energy minima) have been constructed for the homogeneous liquid over a wide temperature range, for the crystal-liquid coexistence state, and for a defective crystalline state. Liquid-phase inherent structures display a vivid polycrystalline character that is strongly obscured by equilibrium thermal motions.

PACS number(s): 05.90.+m, 61.20.Ja, 64.70.Dv

I. INTRODUCTION

Under the influence of simple interparticle interactions, the natural structure for crystalline order in two dimensions is the close-packed triangular array. This is attained experimentally, for example, by electrons on a liquid-helium surface [1], by adsorbed noble-gas atoms floating over an incommensurate substrate [2], and by dense colloidal suspensions confined between parallel glass plates [3]. Theoretical and simulational modeling provide more cases: rigid disks [4], Gaussian cores [5], and Lennard-Jones particles [6] all crystallize in the close-packed triangular pattern in two dimensions.

To attain a comprehensive view of two-dimensional melting phenomena, it is important to examine alternative crystal structures. This paper focuses on the square-crystal case, wherein each particle is symmetrically surrounded by four nearest neighbors (in contrast to six for the close-packed structure). Square arrays have been observed for membrane-spanning bacterial toxin proteins [7] and as planar projections of ordered layers for colloidal suspensions under carefully controlled conditions [8]. They have occasionally been reported to occur as well in simulations of particles with internal degrees of freedom [9,10]. It might also be mentioned in passing that the square crystal provides a two-dimensional analog for the open four-coordinate diamond lattice in three dimensions [11]; alternatively it is analogous to the simple cubic structure observed for the element polonium [12].

Section II describes our model. Molecular-dynamics computer simulation has been used to investigate some aspects of the model's classical equation of state, including melting and freezing phenomena; results are presented in Sec. III. Section IV displays and interprets representative inherent structures (potential-energy minima) for crystal and liquid phases. Finally, Sec. V discusses our findings in the light of recent theory for two-dimensional melting. An Appendix has been included to supply technical details for our treatment of three-body interactions in the molecular-dynamics simulation.

II. MODEL

The particles in our model possess an interaction potential Φ that is composed of two-body and three-body components. Letting λ be a coupling constant for the latter, we have:

$$\Phi(\mathbf{r}_1 \cdots \mathbf{r}_N) = \sum v^{(2)}(r_{ij}) + \lambda \sum v^{(3)}(\mathbf{r}_i, \mathbf{r}_j, \mathbf{r}_k) \ . \tag{2.1}$$

The central pair potential $v^{(2)}$ has been assigned the following form:

$$v^{(2)}(r) = \begin{cases} A\,(r^{-12} - r^{-5}) \exp[(r-a)^{-1}] & (0 < r < a) \\ 0 & (a \le r), \end{cases} \tag{2.2}$$

where

$$A = 6.767\,441, \quad a = 2.464\,918\,32 \ . \tag{2.3}$$

This choice amounts to a finite-range version of the dimensionless Lennard-Jones potential [13]: $v^{(2)}$ vanishes at $r=1$, has a single minimum with unit depth at $r = 2^{1/6}$, and yet smoothly passes to zero at cutoff $r = a$.

In the absence of three-body interactions ($\lambda = 0$), the pair potentials $v^{(2)}$ would once again cause the close-packed triangular crystal to be the classical ground state. But with an appropriate form for $v^{(3)}$ and a sufficiently large coupling strength λ it is possible to stabilize an alternative structure. Without loss of generality one can always write

$$\begin{aligned} v^{(3)}(\mathbf{r}_i, \mathbf{r}_j, \mathbf{r}_k) = {} & h(r_{ij}, r_{ik}, \theta_i) + h(r_{ji}, r_{jk}, \theta_j) \\ & + h(r_{ki}, r_{kj}, \theta_k) \ , \end{aligned} \tag{2.4}$$

where θ_i, for example, represents the vertex angle at particle i in the triangle i,j,k. Then to favor square symmetry about each particle we have set

$$h(r,s,\theta)=\begin{cases}\exp[(r-a_3)^{-1}+(s-a_3)^{-1}]\sin^2(2\theta) & (r,s<a_3),\\ 0 \quad \text{(otherwise)}, & \end{cases} \tag{2.5}$$

where

$$a_3=1.8\ . \tag{2.6}$$

This function is short ranged in distances r and s and in the application considered affects principally nearest neighbors. The trigonometric factor $\sin^2(2\theta)$ vanishes at

$$\theta=0,\pm\pi/2,\pm\pi,\ldots\ , \tag{2.7}$$

but is positive between these angles. Consequently the linear and right-angle triads of neighbors comprised in the square array incur no $v^{(3)}$ penalty, while most triads in the triangular lattice do.

Lattice sums have been evaluated for Φ in the triangular, square, and honeycomb lattices over a wide density range and with the coupling constant range $0\le\lambda\le 30$. At least among these alternatives, the square lattice provides the most stable arrangement if $\lambda>1.7$.

The molecular-dynamics simulations discussed in Sec. III all employ the coupling strength

$$\lambda=5\ . \tag{2.8}$$

Figure 1 graphically exhibits the density dependence of the lattice sums for this λ value. The minimum in the square-lattice curve occurs at the following density ρ and potential energy per particle ϕ:

$$\begin{aligned}\rho_{\min}&=(N/A)_{\min}=0.772\,77\ ,\\ \phi_{\min}&=(\Phi/N)_{\min}=-2.271\,00\ .\end{aligned} \tag{2.9}$$

While this modest search does not absolutely exclude the possibility of other more stable crystals for the given Φ, we find in the simulation discussed below that the system spontaneously selects the square structure as it freezes from the isotropic liquid. We interpret this to be strong evidence that no more stable structure exists for the given interaction.

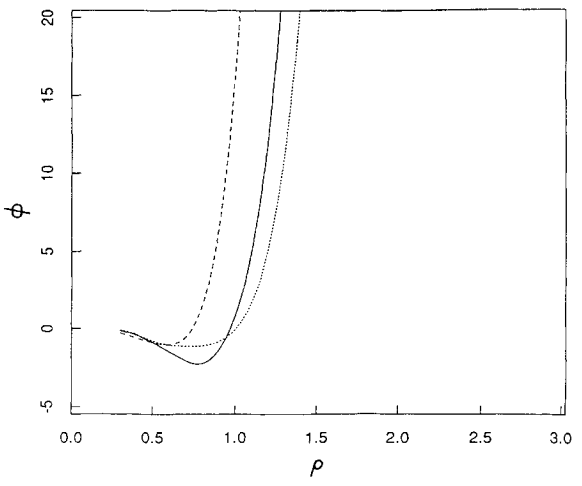

FIG. 1. Potential energy per particle (ϕ) versus reduced density (ρ) for the triangular (dotted line), square (solid line), and honeycomb (dashed line) lattices, with $\lambda=5$.

III. ISOCHORIC EQUATION OF STATE

Our study of the classical statistical mechanics for the square model has relied upon molecular-dynamics computer simulation. The calculations have all involved 2500 particles confined to a square box to which periodic boundary conditions applied. Only a single density has been considered, namely that shown in Eq. (2.9) to give the lowest lattice energy for the square crystal. In this circumstance the box side is

$$L=50(\rho_{\min})^{-1/2}=56.8781\ . \tag{3.1}$$

An unstrained and structurally perfect 50×50 square crystal can reside in the box, oriented so its principle directions are parallel to the box sides, and in registry with its four surrounding periodic images. Of course the boundary conditions permit free translation of the crystal in this orientation.

Owing to the existence of the Pythagorean identity

$$50^2=40^2+30^2\ , \tag{3.2}$$

the unstrained and structurally perfect crystal can equally well adopt either of two alternative rotated configurations. The angles of rotation θ away from the aligned orientation are given by

$$\theta=\pm\arctan(\tfrac{3}{4})\ . \tag{3.3}$$

In these alternatives the square crystal is again in registry with its periodic images. Consequently the classical ground state structurally is threefold degenerate for the chosen particle number and boundary conditions.

The sixth-order Gear algorithm [14] has been used to integrate Newton's equations of motion for the particles, each of which is assigned unit mass. The starting point was the aligned perfect crystal with small random velocities. Temperature was adjusted between runs as usual by scaling velocities. Both heating and cooling sequences of molecular-dynamics runs were generated. By choosing a (reduced) time increment to be 0.002 in all runs, total energy in each run used to evaluate thermodynamic averages remained constant to at worst 1 part in 10^7 (encountered at the high-temperature extreme) and to better than 1 part in 10^8 at low temperature. Thermodynamic state averages were evaluated over runs of 10^4 steps, each of which was preceded by an equilibration run of 2×10^3 steps.

The presence of three-body interactions $v^{(3)}$ in our model presents nontrivial technical complications for the molecular-dynamics simulation procedure and substantially retarded execution speed. By employing identities similar to those advocated by Biswas and Hamann in their silicon modeling study [15], we have been able to relieve this computational bottleneck somewhat. The Appendix provides details of our method, which should be useful in other simulations involving three-body interactions.

Figure 2 shows how the mean value of the potential energy per particle $\langle \Phi \rangle / N$ varies with reduced temperature T^*. The latter is just the mean kinetic energy per particle:

$$T^* = \tfrac{1}{2} \langle (d\mathbf{r}_i/dt)^2 \rangle \ . \tag{3.4}$$

The points plotted in Fig. 2 represent a composite of data from both heating and cooling sequences.

The most striking feature conveyed by Fig. 2 is the sudden rise in $\langle \Phi \rangle / N$ characteristic of a first-order melting transition. This occurs at

$$T_m^* = 0.55 \pm 0.02 \tag{3.5}$$

and involves a melting entropy which we estimate to be

$$\Delta S / k_B = 0.76 \pm 0.05 \ . \tag{3.6}$$

Well below T_m^* the rise in mean potential energy with temperature is very close to the equipartition value expected for independent harmonic phonon modes in the two-dimensional crystal, and indeed that is the state of the system revealed by pictures of instantaneous particle configurations. As T_m^* is approached from below the heat capacity rises slightly above the harmonic base line.

The melting process carries the system directly into an isotropic liquid phase. No evidence has been found for a two-stage melting process of the Kosterlitz-Thouless-Halperin-Nelson-Young (KTHNY) type [16–18] with an intermediate phase exhibiting long-range orientational order but translational disorder. This conclusion is based on observations of the system configuration while passing through T_m^* in both heating and cooling directions. Once melted, further temperature rise above T_m^* causes the heat capacity to decline monotonically from about twice the harmonic normal mode value to substantially less than that value at our upper limit of observation ($T^* \cong 1.8$).

Even though a conventional first-order melting transition appears to be present, three reasons exist why the steeply rising coexistence segment of the curve in Fig. 2 is not strictly vertical. First, our system size (2500 particles) is very small by conventional macroscopic standards. Second, the rate of passage through the transition is not infinitesimal, so slow relaxation processes might lag the thermal control program. Third, the density, rather than pressure, has been held fixed, so that if there were a density change on melting at constant pressure, thermodynamics demonstrates that a melting temperature inter-

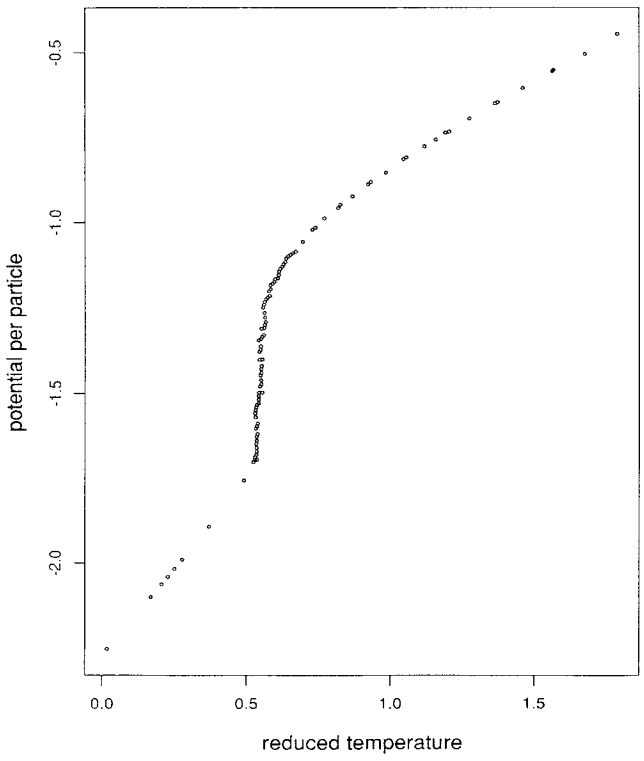

FIG. 2. Mean potential energy per particle ($\langle \Phi \rangle / N$) versus reduced temperature (T^*). The system density is fixed at the value shown in Eq. (2.9).

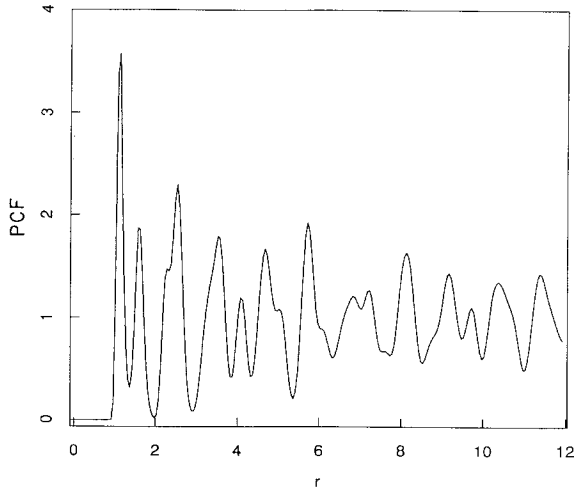

FIG. 3. Particle pair-correlation function for the square-crystal phase at $T^* = 0.491$.

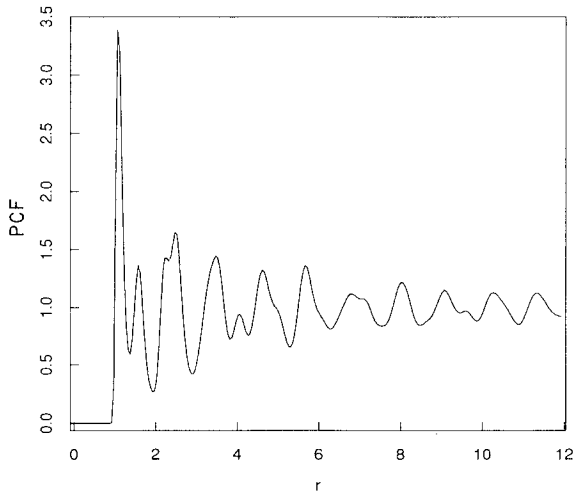

FIG. 4. Particle pair-correlation function for a coexistence state at $T^* = 0.550$.

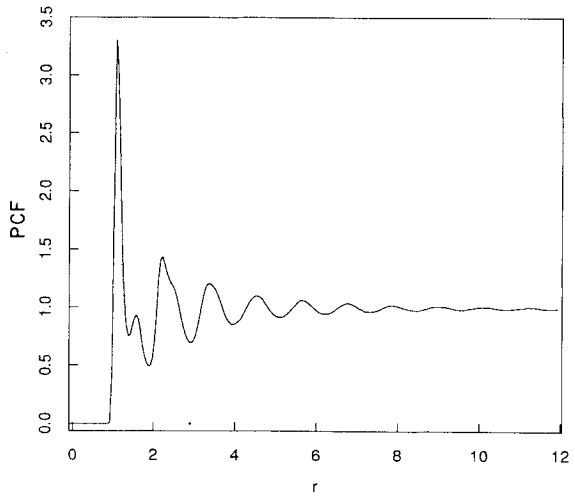

FIG. 5. Particle pair-correlation function for a cool liquid at $T^*=0.588$.

val of phase coexistence should appear with isochoric (constant density) conditions. This last feature is probably a minor consideration for the present model, whose crystal structure is quite open and subject to partial collapse upon melting.

Figures 3–6 present particle pair-correlation functions respectively for a warm but unmelted crystal (at $T^*=0.491$), for a state roughly in the middle of the coexistence interval, for a cool liquid ($T^*=0.588$), and for a hot liquid ($T^*=1.790$). The first of these shows long-range deviations from the function value unity corresponding to uncorrelated particles, with peaks that can be assigned from the coordination geometry of the square lattice. Virtually all of the correlation features present in Fig. 3 can also be identified in the coexistence state, Fig. 4, but with substantially diminished amplitudes. Once the melting process is complete, Fig. 5, spatial decay of positional correlation becomes obvious. Further increasing the temperature, Fig. 6, diminishes the magnitude of local positional order and increases its rate of spatial decay.

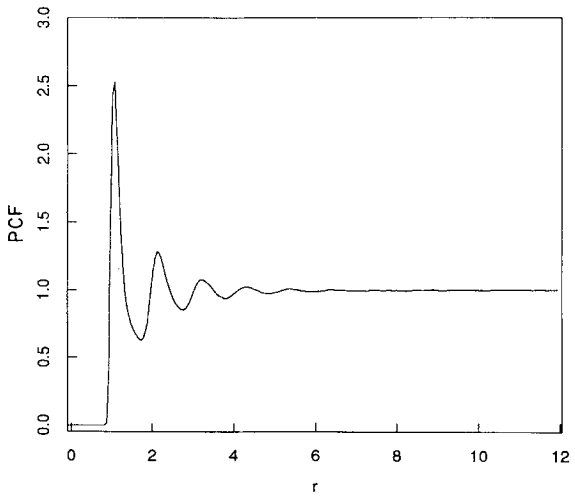

FIG. 6. Particle pair-correlation function for a hot liquid at $T^*=1.790$.

Even at the highest temperatures examined the particle pair-correlation functions display the system's preference for local coordination in the square motif. The short-range order revealed in the first few peaks and valleys appears to be rather different from what is seen in simulations for two-dimensional models with triangular crystalline phases [5,19].

IV. INHERENT STRUCTURES

Theoretical analysis of models for condensed-matter systems can often benefit from construction and classification of the "inherent structures" that are present [13,20]. These are the particle configurations corresponding to the local minima of the model's potential energy function Φ. Arbitrary configurations $\mathbf{r}_1 \cdots \mathbf{r}_N$ (aside from an unimportant zero-measure set) that might be encountered, say, during the course of a molecular-dynamics simulation can be mapped uniquely onto an inherent structure $\mathbf{r}_{1q} \cdots \mathbf{r}_{Nq}$ by solving the coupled set of relaxation equations ($s \geq 0$):

$$\frac{d\mathbf{r}_i(s)}{ds} = -\nabla_i \Phi \quad (i=1,\ldots,N) . \tag{4.1}$$

The solution connecting the initial configuration to an inherent structure describes a steepest-descent pathway on the Φ hypersurface, and the set of initial configurations mapping onto a given inherent structure defines the "basin of attraction" for that inherent structure.

System configurations generated in the low-temperature initial stages of our square-model simulation consist of phonon-distorted, but otherwise perfect, crystal arrangements of the particles. Steepest-descent mapping

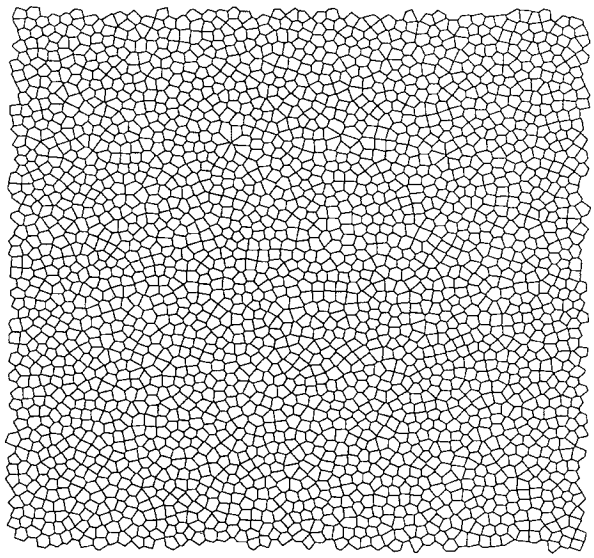

FIG. 7. Nearest-neighbor-polygon representation of the final particle configuration of a hot-liquid run. The temperature was $T^*=1.790$.

simply sets all phonon amplitudes to zero and leaves the system at a global Φ minimum. The result of steepest-descent mapping applied to any one of a representative sample of liquid-state configurations is less obvious; however, the mapping can still be viewed as removal of vibrational amplitude, now in a substantially anharmonic regime [13,20].

Figure 7 shows the particle configuration, in the nearest-neighbor (Voronoi) polygon representation, at the end of our highest-temperature liquid run. This is the $T^*=1.790$ state for which Fig. 6 presented the pair-correlation function. Its random-froth appearance is typical for the liquid phase of our square model. Figure 8 exhibits the corresponding inherent structure, obtained by approximating the solution to Eq. (4.1) by repeatedly setting particle momenta to zero at closely spaced but irregular intervals to avoid the "phonon echo" phenomenon [21]. The change in texture from Fig. 7 to Fig. 8 is both dramatic and revealing: inherent structures underlying at least the hot liquid exhibit a distinctly polycrystalline character.

The particle pair-correlation function has been evaluated for the inherent structure shown in Fig. 8; it appears in Fig. 9. Although only a single system configuration is involved, it seems from our other calculations to be quite representative. Comparison of Fig. 9 with Fig. 6 shows the remarkable enhancement of short-range order that results from removal of intrabasin vibrational distortion. This falls in line with similar observations about inherent structures on a wide variety of model substances [20,22]. The principal peaks in Fig. 9, as expected, correlate with the successive coordination shells of the square crystal. But additionally one observes peak broadening due to frozen-in strains and extra weak features due to the presence of defects.

We have found that inherent structures and their pair-correlation functions produced from other stable liquid states have very similar appearance to those shown in Figs. 8 and 9. This verifies once again that the dominating effect of temperature rise in the stable liquid regime $T^* \geq T_m^*$ (at least under isochoric conditions) is associated with intrabasin vibrational excitation and not with any major shift in the nature of the participating inherent structures [20,22].

Figure 10 presents the final configuration of the coexistence-state run for which Fig. 4 showed the pair-correlation function. Once again the nearest-neighbor cell representation has been used to improve visual clarity. Although interpretation is not without ambiguity, the central portion of the figure from top to bottom appears to contain a single large crystallite. It is flanked on the

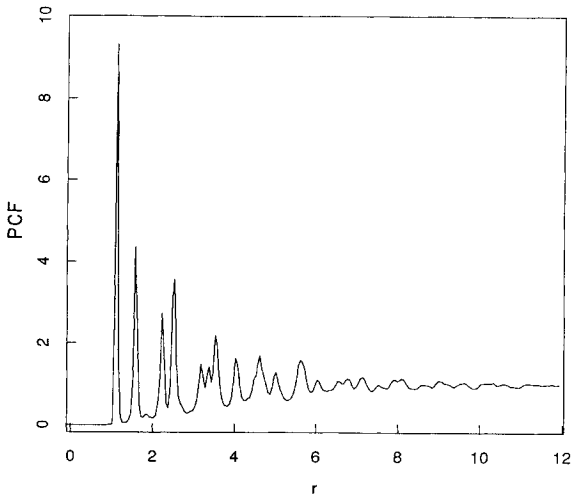

FIG. 9. Particle pair-correlation function for the hot-liquid inherent structure of Fig. 8.

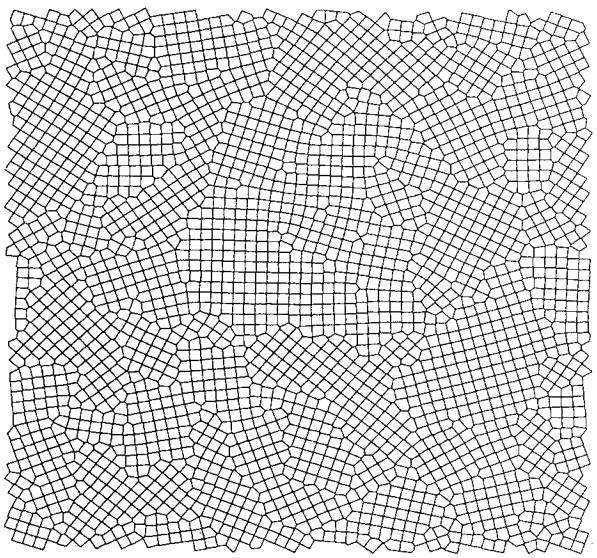

FIG. 8. Inherent structure corresponding to the hot liquid ($T^*=1.790$) configuration of Fig. 7. The nearest-neighbor-polygon representation has been employed for clarity.

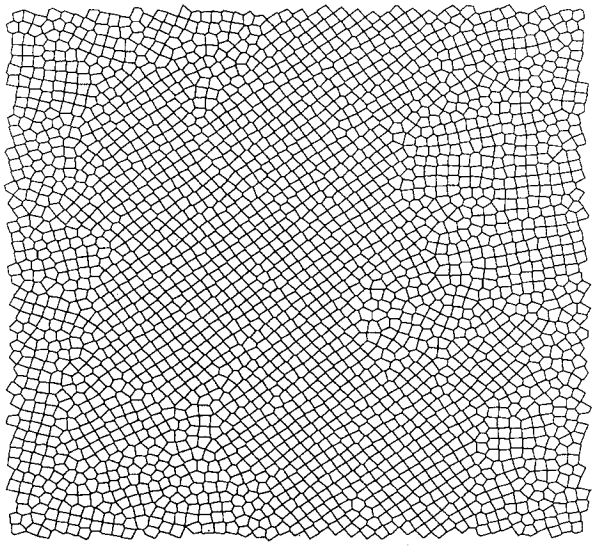

FIG. 10. Particle configuration, in the nearest-neighbor polygon representation, in the coexisting-phase state. The temperature of the run (for which this is the final configuration) was $T^*=0.550$.

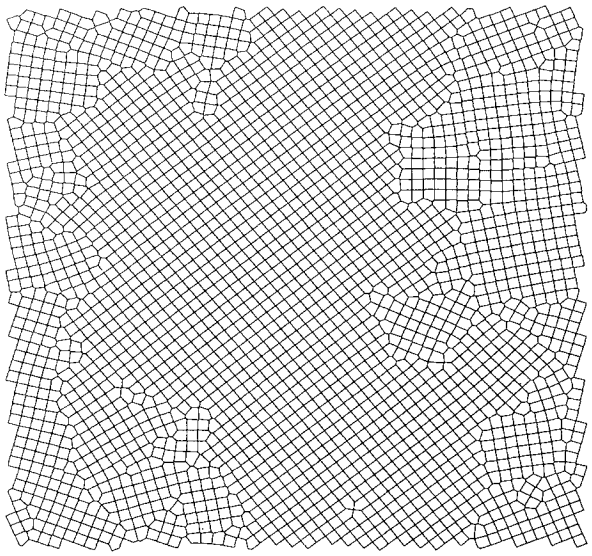

FIG. 11. Inherent structure for the coexisting-phase configuration of Fig. 10.

left and the right by more disordered regions presumably representing for the most part unfrozen liquid.

The inherent structure obtained from the configuration in Fig. 10 appears in Fig. 11. Removal of the distracting influence of intrabasin vibration has substantially eliminated all interpretive ambiguity. The large crystallite spanning the vertical direction and its boundaries have become exceptionally clear. The presence of a monovacancy near the bottom edge of the large crystallite has now become obvious: it produces a cruciform arrangement of four inward-pointing pentagons. Although the crystallite has grown into registered contact with its upper and lower images across the periodic boundaries, notice that it is substantially misoriented with respect to the sides of the primitive cell.

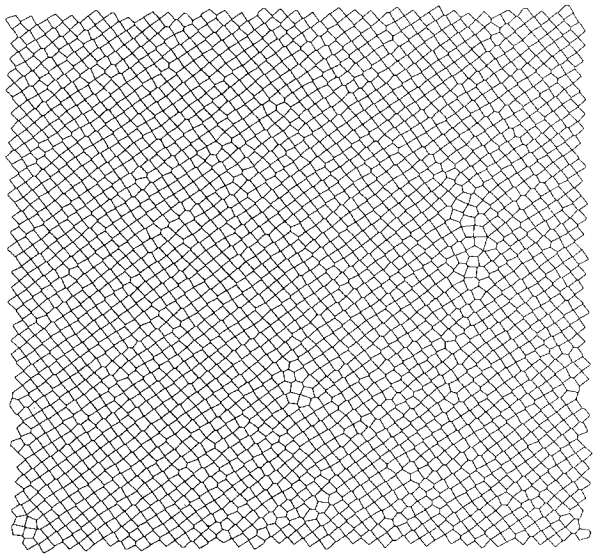

FIG. 12. Particle configuration for a fully refrozen state at $T^*=0.523$.

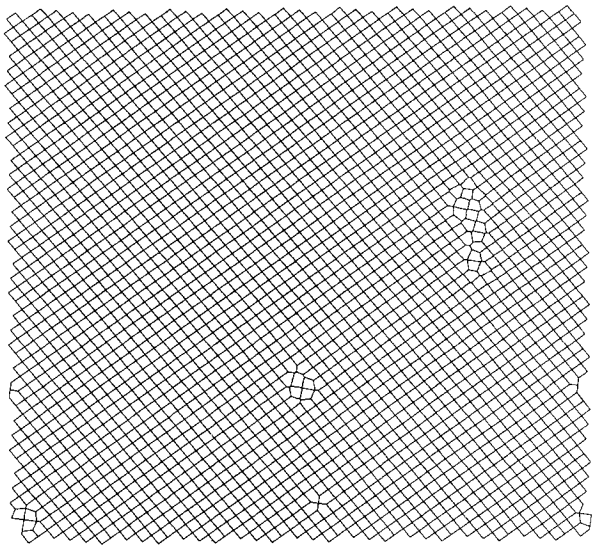

FIG. 13. Inherent structure for the refrozen-state configuration of Fig. 12.

As the slow cooling process that created the coexistence continued, the crystallite grew until it covered the entire system, contacting its periodic images both vertically and horizontally. Figure 12 displays the system configuration at what we took to be essentially the end of the freezing process. Figure 13 shows the corresponding inherent structure and Fig. 14 exhibits its pair-correlation function.

The basic structure shown in Fig. 13 is the rotated crystal described earlier in Sec. III, Eqs. (3.2) and (3.3). However, this frozen sample contains localized defects which did not have an opportunity to anneal out during the finite simulation time. The largest of these defects ap-

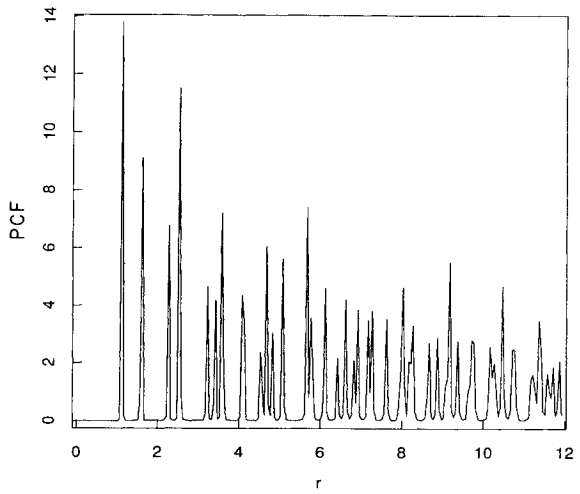

FIG. 14. Particle pair-correlation function for the inherent structure of Fig. 13.

TABLE I. Inherent-structure energies.

Starting state	Final potential energy	Figure number
perfect crystal[a]	−5677.5000	
imperfect rotated crystal	−5632.5290	13
coexistence	−5272.9608	11
cool liquid	−4977.8967	
warm liquid	−4899.2825	
hot liquid	−4899.4102	8

[a]Degenerate aligned and rotated states.

pears near the right-hand side of Fig. 13, slightly closer to the top than to the bottom. After circumscribing this defect with a rectangular boundary of nearest-neighbor cells in the surrounding crystal, and then counting cells within that boundary, one finds that three excess particles have clustered together to form this defect. This is evidence for a strong binding tendency for interstitials embedded in the square crystal.

The "tri-interstitial" represents a local structural collapse, producing a high-density region. It must be compensated by one or more low-density regions. Examination of Fig. 13 in fact reveals that three monovacancies are present. One appears near the vacancy position of Fig. 11, a second (bound to a rotated particle quadruplet) is almost directly above, and the third is at about the same level as the second but split left and right by the periodic boundary conditions. The only other defect structure is an isolated case of a rotated particle quadruplet, fragmented in the view shown between lower left and lower right corners. We believe that these 45°-rotated quadruplets are the square model's lowest energy structural excitations above the crystalline ground state.

Table I shows the values of Φ, the system potential energy, for six inherent structures. These include the perfect crystal, the defective rotated crystal depicted in Fig. 13, the coexistence state (Fig. 11), and three liquid-phase inherent structures. The last two, from molecular-dynamics runs at $T^*=1.156$ and 1.790, respectively, are very close, in spite of having clearly distinct polycrystalline particle arrangements. The cool ($T^*=0.589$) liquid case has a somewhat lower Φ perhaps indicating a modest but real shift in mean inherent structures near the melting point. In any case it is obvious that crystallization produces a far more dramatic lowering of Φ.

V. CONCLUSIONS

By combining two- and three-particle interactions, it has been possible to create a two-dimensional model whose classical ground state (at zero pressure) is a regular square lattice. Molecular-dynamics simulation has been carried out for this model, with 2500 particles subject to periodic boundary conditions and constant system area. A consistent conclusion from both heating and cooling sequences, with spontaneous melting and freezing events, is that the square lattice remains the only stable crystal form up to the melting point.

Inherent structures (particle configurations corresponding to local potential-energy minima) have been constructed for solid-, liquid-, and coexisting-phase states. Those produced from representative system samples in the liquid phase display a polycrystalline texture and except just above the melting point appear to be largely independent of the starting temperature.

The simulational evidence seems only to be consistent with a conventional first-order melting transition, with the square crystal phase passing directly into isotropic liquid. The melting entropy [Eq. (3.6)] is relatively large for two-dimensional melting of structureless-particle systems [4,23].

No evidence has been uncovered for the presence of an orientationally ordered, translationally disordered phase interposed between the square crystal and the isotropic liquid: the refrozen crystal (Fig. 13) is devoid of isolated dislocations. Such a possibility is inferentially suggested by the KTHNY theory of two-dimensional melting [15–18] and in the present circumstance presumably would lead to a "quadratic" phase with fourfold bond orientational order, analogous to the more conventionally discussed "hexatic" order. Nevertheless it remains possible that by changing the system density and/or varying the coupling constant λ for the three-particle interactions in our model that two-stage melting of the KTHNY type might be produced. In any case it is important to note that KTHNY theory requires extension to cover the present case, since square crystals have three independent elastic constants, compared to two for triangular crystals.

The polycrystalline character of the inherent structures underlying the liquid phase for our model is not without precedent. Udink [24] has produced analogous textures for the liquid-phase inherent structures of the two-dimensional Lennard-Jones system. Furthermore it is known that in the $n\rightarrow\infty$ limit for pair interactions $(\sigma/r_{ij})^n$ that inherent structures correspond to rigid sphere ($D=3$) or disk ($D=2$) packings [25] and that random disk packings have a polycrystalline character [26,27]. This leads one to suspect that a similar situation would obtain in the case of honeycomb-lattice systems; our three-particle interaction could be modified to stabilize this threefold coordination geometry and then could be simulated as described above.

APPENDIX

Three-body interactions $v^{(3)}$ in the system's potential energy Φ, Eq. (2.1), nominally require a threefold summation. For large numbers N of particles this would appear to present a substantial computational bottleneck. However, the specific form (2.4) and (2.5) selected for $v^{(3)}$ can easily be shown to produce a reduction to twofold summation. This fortunate circumstance enhances the utility of such interaction in the simulation of large systems.

The sum of three-body terms may be expressed

$$\sum_{i,j,k} v^{(3)}(\mathbf{r}_i,\mathbf{r}_j,\mathbf{r}_k) = \tfrac{1}{2}\sum_i \sum_{j,k} (1-\delta_{ij})(1-\delta_{ik})h(r_{ij},r_{ik},\theta_i) \quad \text{(A1)}$$

since

$$h(r_{ij},r_{ij},\theta_i)\equiv h(r_{ij},r_{ij},0)=0 .$$

Equation (2.5) can be written as follows:

$$h(r_{ij},r_{ik},\theta_i)=\tfrac{1}{4}f_3(r_{ij})f_3(r_{ik})\sin^2(2\theta_i) , \tag{A2}$$

where

$$f_3(r)=\begin{cases}2\exp[(r-a_3)^{-1}] & (0\le r<a_3)\\ 0 & (a_3\le r).\end{cases} \tag{A3}$$

We can now transform Eq. (A2) to

$$\begin{aligned}h(r_{ij},r_{ik},\theta_i)=&[\tilde{x}_{ij}^2\tilde{y}_{ij}^2+\tilde{x}_{ik}^2\tilde{y}_{ik}^2-8\tilde{x}_{ij}^2\tilde{y}_{ij}^2\tilde{x}_{ik}^2\tilde{y}_{ik}^2\\ &-2\tilde{x}_{ij}\tilde{y}_{ij}\tilde{x}_{ik}\tilde{y}_{ik}(\tilde{x}_{ij}^2-\tilde{y}_{ij}^2)(\tilde{x}_{ik}^2-\tilde{y}_{ik}^2)]\\ &\times f_3(r_{ij})f_3(r_{ik}) ,\end{aligned} \tag{A4}$$

where $\tilde{x}_{ij}=x_{ij}/r_{ij}$, etc. If we define two additional functions as follows:

$$g_3(\mathbf{r}_{ij})=\tilde{x}_{ij}^2\tilde{y}_{ij}^2 f_3(r_{ij}) , \tag{A5}$$

$$h_3(\mathbf{r}_{ij})=\tilde{x}_{ij}\tilde{y}_{ij}(\tilde{x}_{ij}^2-\tilde{y}_{ij}^2)f_3(r_{ij}) , \tag{A6}$$

then Eq. (A4) becomes

$$\begin{aligned}h(r_{ij},r_{ik},\theta_i)=&g_3(\mathbf{r}_{ij})f_3(r_{ik})+f_3(r_{ij})g_3(\mathbf{r}_{ik})\\ &-8g_3(\mathbf{r}_{ij})g_3(\mathbf{r}_{ik})-2h_3(\mathbf{r}_{ij})h_3(\mathbf{r}_{ik}) .\end{aligned} \tag{A7}$$

Next introduce three new quantities

$$F_i=\sum_j(1-\delta_{ij})f_3(r_{ij}) , \tag{A8}$$

$$G_i=\sum_j(1-\delta_{ij})g_3(\mathbf{r}_{ij}) , \tag{A9}$$

$$H_i=\sum_j(1-\delta_{ij})h_3(\mathbf{r}_{ij}) . \tag{A10}$$

Using these, Eqs. (A1) and (A7) immediately simplify to

$$\sum_{i,j,k}v^{(3)}(\mathbf{r}_i,\mathbf{r}_j,\mathbf{r}_k)=\sum_i(F_iG_i-4G_i^2-H_i^2) . \tag{A11}$$

The structure of Eqs. (A8)–(A11) make it clear that only double sums are required to evaluate the three-body potential energy.

This generic technique may be used for any three-body potential which is a product of radial functions and polynomials of angle sine and cosine quantities. A similar decomposition may be effected when several atomic species are present; in that case the analogs of F_i, G_i, and H_i would be sets of quantities involving summation only over atoms j of a single species.

[1] C. G. Grimes and G. A. Adams, Phys. Rev. Lett. **42**, 795 (1979).

[2] P. A. Heiney, R. J. Birgenau, G. S. Brown, P. M. Horn, D. E. Moncton, and P. W. Stephens, Phys. Rev. Lett. **48**, 104 (1982).

[3] C. A. Murray and D. H. Van Winkle, Phys. Rev. Lett. **58**, 1200 (1987).

[4] B. J. Alder and T. E. Wainwright, Phys. Rev. **127**, 359 (1962).

[5] F. H. Stillinger and T. A. Weber, J. Chem. Phys. **74**, 4015 (1981); T. A. Weber and F. H. Stillinger, *ibid.* **74**, 4020 (1981).

[6] F. F. Abraham, Phys. Rev. B **23**, 6145 (1981).

[7] I. Amato, Science **255**, 684 (1992).

[8] D. H. Van Winkle and C. A. Murray, Phys. Rev. A **34**, 562 (1986).

[9] P. N. Kusalik and S. F. O'Shea, Mol. Phys. **49**, 33 (1983).

[10] D. Marx, P. Nielaba, and K. Binder, Phys. Rev. Lett. **67**, 3124 (1991).

[11] G. H. Wannier, *Elements of Solid State Theory* (Cambridge University Press, New York, 1959), p. 32.

[12] J. Donohue, *The Structures of the Elements* (Krieger, Malabar, FL, 1982), p. 391.

[13] (a) F. H. Stillinger and T. A. Weber, Phys. Rev. A **28**, 2408 (1983); (b) R. A. LaViolette and F. H. Stillinger, J. Chem. Phys. **83**, 4079 (1985).

[14] H. J. C. Berendsen and W. F. van Gunsteren, in *Molecular Dynamics Simulation of Statistical-Mechanical Systems,* edited by G. Ciccotti and W. G. Hoover (North-Holland, Amsterdam, 1986), pp. 52–55.

[15] R. Biswas and D. Hamann, Phys. Rev. B **36**, 6434 (1987).

[16] J. M. Kosterlitz and D. J. Thouless, J. Phys. C **6**, 1181 (1973).

[17] D. R. Nelson and B. I. Halperin, Phys. Rev. B **19**, 2457 (1979); D. R. Nelson, in *Phase Transitions and Critical Phenomena,* edited by C. Domb and J. L. Lebowitz (Academic, London, 1983), Vol. 7.

[18] A. P. Young, Phys. Rev. B **19**, 1855 (1979).

[19] J. Q. Broughton, G. H. Gilmer, and J. D. Weeks, Phys. Rev. B **25**, 4651 (1982).

[20] F. H. Stillinger and T. A. Weber, Phys. Rev. A **25**, 978 (1982); Science **225**, 983 (1984); F. H. Stillinger, in *Mathematical Frontiers in Computational Chemical Physics,* edited by D. G. Truhlar (Springer-Verlag, New York, 1988).

[21] G. S. Grest, S. R. Nagel, and A. Rahman, Solid State Commun. **36**, 875 (1980).

[22] F. H. Stillinger and T. A. Weber, J. Chem. Phys. **80**, 4434 (1984); T. A. Weber and F. H. Stillinger, *ibid.* **81**, 5089 (1984); F. H. Stillinger and T. A. Weber, Phys. Rev. B **31**, 5262 (1985); J. Chem. Phys. **88**, 5123 (1988); T. A. Weber and F. H. Stillinger, *ibid.* **95**, 3614 (1991).

[23] F. van Swol, L. V. Woodcock, and J. N. Cape, J. Chem. Phys. **73**, 913 (1980).

[24] C. Udink, doctoral thesis, University of Amsterdam, 1987.

[25] F. H. Stillinger and T. A. Weber, J. Chem. Phys. **83**, 4767 (1985).

[26] B. D. Lubachevsky and F. H. Stillinger, J. Stat. Phys. **60**, 561 (1990).

[27] B. D. Lubachevsky, F. H. Stillinger, and E. N. Pinson, J. Stat. Phys. **64**, 501 (1991).